SCIENCE CHINA
Information Sciences

• RESEARCH PAPER •

May 2025, Vol. 68, Iss. 5, 150305:1–150305:17
https://doi.org/10.1007/s11432-024-4375-4

Special Topic: Integrated Sensing and Communications Techniques for 6G

# Resolution-aware beam scanning for joint detection and communication in ISAC systems

Yiming XU[1], Dongfang XU[1*], Zhanyuan XIE[2], Zheng JIANG[2], Shenghui SONG[1] & Derrick Wing Kwan NG[3]

[1]*Department of Electronic and Computer Engineering, The Hong Kong University of Science and Technology, Hong Kong 999077, China*
[2]*China Telecom Research Institute, Beijing 100191, China*
[3]*School of Electrical Engineering and Telecommunications, University of New South Wales, Sydney 1466, Australia*

Received 31 October 2024/Revised 18 February 2025/Accepted 2 April 2025/Published online 23 April 2025

**Abstract** Beam scanning for joint detection and communication in integrated sensing and communication (ISAC) systems plays a critical role in continuous monitoring and rapid adaptation to dynamic environments. However, the design of sequential scanning beams for target detection with the required sensing resolution has not been tackled in the literature. To bridge this gap, this paper introduces a resolution-aware beam scanning design. In particular, the transmit information beamformer, the covariance matrix of the dedicated radar signal, and the receive beamformer are jointly optimized to maximize the average sum rate of the system while satisfying the sensing resolution and detection probability requirements. A block coordinate descent (BCD)-based optimization framework is developed to address the non-convex design problem. By exploiting successive convex approximation (SCA), S-procedure, and semidefinite relaxation (SDR), the proposed algorithm is guaranteed to converge to a stationary solution with polynomial time complexity. Simulation results show that the proposed design can efficiently handle the stringent detection requirement and outperform existing antenna-activation-based methods in the literature by exploiting the full degrees of freedom (DoFs) brought by all antennas.

**Keywords** integrated sensing and communication (ISAC), detection, beam scanning, resolution, beamwidth

**Citation** Xu Y M, Xu D F, Xie Z Y, et al. Resolution-aware beam scanning for joint detection and communication in ISAC systems. Sci China Inf Sci, 2025, 68(5): 150305, https://doi.org/10.1007/s11432-024-4375-4

## 1 Introduction

Integrated sensing and communication (ISAC) has been widely recognized as a promising technology for enabling the future sixth-generation (6G) wireless networks to support various emerging applications, including environment monitoring, autonomous driving, unmanned aerial vehicles (UAVs), and vehicular networks [1–4]. As a result, plenty of research has been conducted on performance analysis and system design for ISAC systems, such as performance characterization [5, 6], resource allocation [7–9], and waveform design [10–12]. However, there are still numerous challenges that need to be tackled to fully unlock the potential of ISAC systems.

Target detection is one of the essential tasks explored in various ISAC scenarios, e.g., joint target detection and near-field communication [13] and eavesdropper detection for physical layer security (PLS) design [14]. However, most existing methods require prior information about the target, which is challenging to obtain in practice. To tackle this issue, the authors of [15–17] proposed to scan the monitored area for target detection and serve the communication users simultaneously. Beam scanning involves steering a focused beam of electromagnetic energy across a region of interest to identify, locate, and track targets [18]. This process enhances spatial coverage. Specifically, by systematically scanning the beam over multiple angles, the system can ensure that all regions of interest are explored, reducing the likelihood of missing a target. In addition, beam scanning enables the tracking of moving targets by monitoring changes in their positions over successive beam sweeps. Finally, beam scanning offers higher spatial resolution by constructing narrower beams and minimizing the potential overlap between adjacent

* Corresponding author (email: eedxu@ust.hk)

 

regions. The authors of [19, 20] proposed to jointly design the resource allocation among all scanning sectors to improve the system performance. Specifically, Xu et al. [19] jointly optimized the resources over a sequence of variable-length snapshots, generating dedicated scanning beams, to detect the targets while serving communication users. The information beamformer and artificial noise over all snapshots, as well as the duration of each snapshot, are jointly optimized to maximize the sum secrecy rate. Furthermore, Wang et al. [20] studied an ISAC system that achieves 360° radar detection and directional communication simultaneously. The detection probability of all sectors is maximized while guaranteeing the communication coverage probability in each sector.

Although significant progress has been made, designing scanning beams to differentiate closely located targets with a given resolution requirement remains an open problem. The difficulty arrives from the constraints on the beamwidth for each scanning beam. To this end, several beamwidth controlling algorithms have been proposed [21–23]. In specificity, Pang et al. [21] considered UAV-enabled vehicular networks, where the UAV dynamically adjusts the transmit beamwidth to cover the moving vehicle. Also, Du et al. [22] proposed to use the wide beamwidth to obtain the direction of the vehicle, followed by the narrow beamwidth to achieve efficient communication in vehicle-to-infrastructure (V2I) systems. In particular, the time-splitting ratio between the wide and narrow beamwidth was optimized to maximize the achievable rate. Moreover, Bai et al. [23] proposed to control the beamwidth to achieve an energy-efficient design in UAV-aided ISAC systems. Nevertheless, existing methods control the beamwidth by adapting the number of activated antennas, which do not utilize the full spatial degrees of freedom (DoFs).

In this paper, we propose a resolution-aware beam scanning scheme. In particular, we divide the monitored area into multiple sectors in the angular domain, where the angular width of each sector is determined by the resolution requirements. For beam scanning in each sector, the base station (BS) generates high-directional beams to detect the potential target in the sector and serve the communication users at the same time. Different from existing methods, e.g., [21–23], that control the beamwidth by activating different numbers of antennas, we design the beam pattern to match the ideal beampattern.

The main contributions of this paper are summarized as follows.

- We investigate the resolution-aware beam scanning design for joint detection and communication, where the sequential scanning beams are jointly designed with given resolution requirements. The average sum rate is maximized while guaranteeing the sensing resolution and detection probability requirements by jointly optimizing the transmit information beamformer, the covariance matrix of the dedicated radar signal, and the receive beamformer of all sectors.
- To handle the non-convex design problem with coupled variables and complicated expressions in the objective function, we develop an optimization framework based on the block coordinate descent (BCD) algorithm to achieve a stationary solution with polynomial time complexity. Specifically, we first derive the optimal expression for the receive beamformer and substitute it into detection constraint to eliminate the coupling issue with the receive beamformer. Then, successive convex approximation (SCA) is employed to address the detection constraint. Subsequently, we apply series transformations to make the objective function tractable and then explore S-procedure to solve the semi-infinite programming caused by the imperfect channel state information (CSI). Finally, the optimization variables are divided into two blocks and handled by the BCD algorithm.
- The effectiveness of the proposed scheme is validated by simulation results. It is observed that the proposed scheme is able to satisfy stringent detection requirements with almost no impact on communication performance. Moreover, compared with the existing studies that control the beamwidth by adapting the activated number of antennas, approximating the beampattern to the ideal resolution-dependent beampattern in the proposed scheme does not sacrifice the design DoFs and achieves significant performance improvement.

**Notations.** Vectors and matrices are denoted by boldface lowercase and boldface capital letters, respectively. $\mathbb{R}^{M\times N}$ and $\mathbb{C}^{M\times N}$ represent the space of the $M\times N$ real-valued and complex-valued matrices, respectively. $|\cdot|$ and $||\cdot||_2$ denote the absolute value of a complex scalar and the $l_2$-norm of a vector, respectively. $\mathbb{H}^N$ denotes the set of complex Hermitian matrices of dimension $N$. $(\cdot)^{\mathrm{T}}$ and $(\cdot)^{\mathrm{H}}$ stand for the transpose and the conjugate transpose operator, respectively. $\boldsymbol{I}_N$ refers to the $N$ by $N$ identity matrix. $\mathrm{Tr}(\boldsymbol{A})$ and $\mathrm{Rank}(\boldsymbol{A})$ denote the trace and the rank of matrix $\boldsymbol{A}$, respectively. $\boldsymbol{A}\succeq\boldsymbol{0}$ indicates that $\boldsymbol{A}$ is a positive semidefinite matrix. $\Re\{\cdot\}$ and $\Im\{\cdot\}$ represent the real and imaginary parts of a complex number, respectively. Vectorization of matrix $\boldsymbol{A}$ is denoted by $\mathrm{vec}(\boldsymbol{A})$, and $\boldsymbol{A}\otimes\boldsymbol{B}$ represents the Kronecker product between two matrices $\boldsymbol{A}$ and $\boldsymbol{B}$. $\mathbb{E}[\cdot]$ refers to statistical expectation.

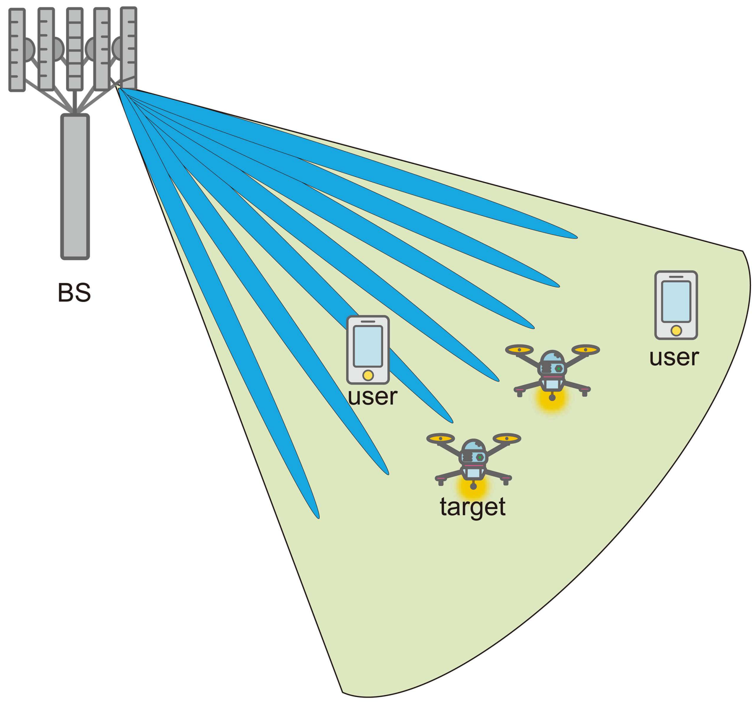


**Figure 1** (Color online) Illustration of the considered resolution-aware beam scanning ISAC system.

$\triangleq$ and $\sim$ stand for "defined as" and "distributed as", respectively. $\mathcal{CN}(0, \sigma^2)$ denotes the distribution of a circularly symmetric complex Gaussian random variable with mean 0 and variance $\sigma^2$. $\mathcal{O}(\cdot)$ is the big-O notation. The gradient vector of function $f(\boldsymbol{x})$ with respect to $\boldsymbol{x}$ is denoted as $\nabla_{\boldsymbol{x}} f(\boldsymbol{x})$.

## 2 System model

As shown in Figure 1, we consider an ISAC system with one BS and $K$ communication users. The BS is equipped with a uniform linear array (ULA) consisting of $N$ antennas, while $K$ users are single-antenna devices[1)]. We place the center of the ULA at the origin of the reference frame and align the ULA parallel to the $x$-axis. The BS performs sequential beam scanning for target detection and communication with the desired users at the same time. To distinguish the targets at a distance, the beamwidth of the transmitted signal should be small enough to separate the targets, which imposes the angular resolution requirement on the scanning beams [24]. To achieve the specific angular resolution, we divide the whole monitored area into $L$ non-overlapped sectors in the angular domain, and the BS scans the area with a sequence of $L$ beams[2)]. For notation simplicity, we define the sets $\mathcal{K} \triangleq \{1, \ldots, K\}$ and $\mathcal{L} \triangleq \{1, \ldots, L\}$ to collect the indices for communication users and sectors, respectively.

To achieve effective joint detection and communication, the transmitted dual-functional radar-communication (DFRC) signal of the BS at sector $l \in \mathcal{L}$, is given by

$$\boldsymbol{x}[l] = \sum_{k \in \mathcal{K}} \boldsymbol{w}_k[l] s_k[l] + \boldsymbol{r}[l], \tag{1}$$

where $\boldsymbol{w}_k[l] \in \mathbb{C}^N$ denotes the beamforming vector for user $k$ and $s_k \sim \mathcal{CN}(0, 1)$ denotes the information signal for user $k$. $\boldsymbol{r}[l] \in \mathbb{C}^N$ is the dedicated sensing signal for sector $l$ and is assumed to be independent with information signals [25]. $\boldsymbol{r}[l]$ is assumed to follow the complex Gaussian distribution with $\mathcal{CN}(\boldsymbol{0}, \boldsymbol{R}[l])$, where $\boldsymbol{R} \in \mathbb{H}^N$ is the radar covariance matrix of $\boldsymbol{r}[l]$. Then, the covariance of the

1) ULA has been utilized to investigate the resolution-aware beam control in literature, e.g., [21, 23]. To achieve better angular resolution, uniform planar array (UPA) can be adopted by modifying the channel model accordingly.

2) In practice, we can set $L$ according to the maximum tolerable detection resolution to strike an effective balance between target detection resolution and system complexity.

transmitted signal $\boldsymbol{x}[l]$ is given by

$$\boldsymbol{S}[l] \triangleq \mathbb{E}\left[\boldsymbol{x}[l]\boldsymbol{x}^{\mathrm{H}}[l]\right] = \sum_{k\in\mathcal{K}} \boldsymbol{w}_k[l]\boldsymbol{w}_k^{\mathrm{H}}[l] + \boldsymbol{R}[l]. \tag{2}$$

### 2.1 Received communication signal

The received signal of user $k$ at sector $l$ is given by

$$\begin{aligned} y_k[l] = &\ \boldsymbol{h}_k^{\mathrm{H}}\boldsymbol{x}[l] + n_k \\ = &\ \underbrace{\boldsymbol{h}_k^{\mathrm{H}}\boldsymbol{w}_k[l]s_k[l]}_{\text{Desired information signal}} + \underbrace{\boldsymbol{h}_k^{\mathrm{H}}\boldsymbol{r}[l]}_{\text{Interference from sensing signal}} \\ &+ \underbrace{\sum_{k'\in\mathcal{K}\setminus\{k\}} \boldsymbol{h}_k^{\mathrm{H}}\boldsymbol{w}_{k'}[l]s_{k'}}_{\text{Multiuser interference}} + n_k, \end{aligned} \tag{3}$$

where $\boldsymbol{h}_k \in \mathbb{C}^N$ is the channel vector between the BS and user $k$, and $n_k \sim \mathcal{CN}(0, \sigma_k^2)$ denotes the additive white Gaussian noise (AWGN) at user $k$.

The CSI of different users is acquired at the beginning of the scanning period to achieve the joint design of scanning beams. However, in the sequential beam scanning period, the CSI may vary due to the dynamic environment, such as the moving targets [19]. Thus, we adopt the widely used bounded CSI error model [26], which is given by

$$\boldsymbol{h}_k = \overline{\boldsymbol{h}}_k + \Delta\boldsymbol{h}_k,\ \Delta\boldsymbol{h}_k \in \Omega_k, \tag{4}$$

where $\overline{\boldsymbol{h}}_k \in \mathbb{C}^N$ is the estimated channel of user $k$ and $\Delta\boldsymbol{h}_k \in \mathbb{C}^N$ denotes the corresponding CSI uncertainty. $\Omega_k$ is the uncertainty set given by

$$\Omega_k \triangleq \left\{\Delta\boldsymbol{h}_k \in \mathbb{C}^N \mid \|\Delta\boldsymbol{h}_k\|_2 \leqslant \beta_k\right\}, \tag{5}$$

where $\beta_k$ is the norm bounded error of $\Delta\boldsymbol{h}_k$. In practice, $\beta_k$ can be estimated through field measurements [27] and machine learning techniques [28].

### 2.2 Received sensing signal

The received echoes at the BS of the sector $l$ is given by

$$\boldsymbol{y}_s[l] = \alpha_t\varrho_t\boldsymbol{a}(\phi_l)\boldsymbol{a}^{\mathrm{H}}(\phi_l)\boldsymbol{x}[l] + \sum_{m\in\mathcal{M}} \alpha_m\varrho_m\boldsymbol{a}(\psi_m)\boldsymbol{a}^{\mathrm{H}}(\psi_m)\boldsymbol{x}[l] + \boldsymbol{n}_s[l], \tag{6}$$

where $\mathcal{M} \triangleq \{1,\ldots,M\}$ denote the set to collect the indices of $M$ clutters. $\alpha_t \sim \mathcal{CN}(0,\sigma_t^2)$ and $\alpha_m \sim \mathcal{CN}(0,\sigma_m^2)$ are radar cross section (RCS) coefficients for the target and clutter $m$, respectively [29, 30]. $\varrho_t = (\frac{\lambda_c}{4\pi d^{\varsigma_s}})^2$ and $\varrho_m = (\frac{\lambda_c}{4\pi d_m^{\varsigma_s}})^2$ denote distance-dependent pathloss with $\lambda_c$ being the wavelength of the carrier and $\varsigma_s$ being the pathloss exponent for the sensing channel. $d$ and $d_m$ denote the distance from the BS to the target and clutter $m$, respectively. $\phi_l$ represents the central direction of the sector $l$, and $\psi_m$ is the direction of the clutter $m$. $\boldsymbol{n}_s[l] \sim (\boldsymbol{0}, \sigma_s^2\boldsymbol{I}_N)$ denotes the AWGN at the BS and $\boldsymbol{a}(\theta)$ represents the steering vector in direction $\theta$ given by

$$\boldsymbol{a}(\theta) \triangleq [1, \mathrm{e}^{\mathrm{j}\pi\cos\theta}, \ldots, \mathrm{e}^{\mathrm{j}\pi(N-1)\cos\theta}]^{\mathrm{T}}, \tag{7}$$

where the antenna spacing is half-wavelength.

## 3 Performance metrics and problem formulation

### 3.1 Performance metrics

#### 3.1.1 *Performance metrics for communication*

According to (3), the signal-to-interference-plus-noise ratio (SINR) of user $k$ at sector $l$ is given by

$$\gamma_k[l] = \frac{\left|\boldsymbol{h}_k^{\mathrm{H}}\boldsymbol{w}_k[l]\right|^2}{\sum_{k'\in\mathcal{K}\setminus\{k\}} \left|\boldsymbol{h}_k^{\mathrm{H}}\boldsymbol{w}_{k'}[l]\right|^2 + \boldsymbol{h}_k^{\mathrm{H}}\boldsymbol{R}[l]\boldsymbol{h}_k + \sigma_k^2}. \tag{8}$$

The corresponding achievable rate of user $k$ is given by

$$R_k[l] = \log_2 \left(1 + \gamma_k[l]\right), \ (\text{bits/s/Hz}). \tag{9}$$

#### 3.1.2 *Performance metrics for sensing*

**(1) Beam scanning.** To distinguish two targets with the distance of $\Delta d$ in the azimuth direction at a distance $d$, the required beamwidth $\Delta\theta$ is given by [31]

$$\Delta\theta = 2 \arcsin \frac{\Delta d}{2d}. \tag{10}$$

Then, the angular width of each sector should not be larger than $\Delta\theta$. Accordingly, the number of required sectors for beam scanning is determined by $L = \left\lceil \frac{\Delta\theta_{\text{area}}}{\Delta\theta} \right\rceil$, where $\theta_{\text{area}}$ is the angular width of the monitored area and $\lceil\cdot\rceil$ represents the operation of round-up to the nearest integer. To illuminate the sector and suppress the side lobe energy leakage to the other sectors, the ideal beampattern for sector $l$ is given by

$$P_l(\theta_i) = \begin{cases} 1, & |\theta_i - \phi_l| \leqslant \dfrac{\Delta\theta}{2}, \\ 0, & \text{otherwise}, \end{cases} \quad \forall i \in \mathcal{I}, \tag{11}$$

where we quantize the angular domain $[0, 2\pi]$ into $I$ possible directions and denote the set $\mathcal{I} \triangleq [1, \ldots, I]$ to collect the quantized direction indices. $\theta_i$ denotes the angle corresponding to the $i$-th quantized direction. Since the target detection task aims to detect the existence of unknown targets in all sectors, the beampattern design holds for all $l \in \mathcal{L}$.

However, the ideal beampattern is hard to generate in practice. To this end, the beampattern matching error is considered as a metric to restrict the generated beampattern to approximately match the ideal beampattern $P_l(\theta_i)$ [32]. With the transmitted signal $\boldsymbol{x}[l]$, the beampattern gain for sector $l$ at direction $\theta_i$ is given by

$$\begin{aligned} P_l^*(\theta_i) &= \mathbb{E}\left[\left|\boldsymbol{a}^{\mathrm{H}}(\theta_i)\boldsymbol{x}[l]\right|^2\right] \\ &= \boldsymbol{a}^{\mathrm{H}}(\theta_i)\left(\sum_{k\in\mathcal{K}} \boldsymbol{w}_k[l]\boldsymbol{w}_k^{\mathrm{H}}[l] + \boldsymbol{R}[l]\right)\boldsymbol{a}(\theta_i). \end{aligned} \tag{12}$$

Then, the beampattern matching error for sector $l$ is given by

$$\mathcal{E}_l\left(\{\boldsymbol{w}_k[l]\}, \boldsymbol{R}[l], \xi[l]\right) = \frac{1}{I}\sum_{i\in\mathcal{I}} \left|P_l^*(\theta_i) - \xi[l]P_l(\theta_i)\right|^2, \tag{13}$$

where $\xi[l]$ is the scaling factor to be optimized [33].

**Remark 1.** In scenarios where two targets are located closely within the same sector, the BS may struggle to differentiate them. To handle this issue, we can periodically shift the angular interval of the sectors to make the targets separable by different sectors [34]. For example, denote the angular range of the $l$-th sector in one round of beam scanning as $(\psi_l, \hat{\psi}_l)$. Then, for the next round of beam scanning, the angular range of the $l$-th sector can be shifted to $(\psi_l + \delta, \hat{\psi}_l + \delta)$. With this angular shift, it is possible to separate the closely located targets for a given $\delta$.

**(2) Target detection.** With the divided scanning sectors, target detection is performed in each sector. By applying the receive beamformer $\boldsymbol{u}[l] \in \mathbb{C}^N$ for sector $l$ on the echoes in (6), the resulting signal is given by

$$\begin{aligned} y_s[l] &= \boldsymbol{u}^{\mathrm{H}}[l]\boldsymbol{y}_s[l] \\ &= \alpha_t \varrho_t \boldsymbol{u}^{\mathrm{H}}[l]\boldsymbol{a}(\phi_l)\boldsymbol{a}^{\mathrm{H}}(\phi_l)\boldsymbol{x}[l] + \boldsymbol{u}^{\mathrm{H}}[l]\sum_{m\in\mathcal{M}} \alpha_m \varrho_m \boldsymbol{a}(\psi_m)\boldsymbol{a}^{\mathrm{H}}(\psi_m)\boldsymbol{x}[l] + \boldsymbol{u}^{\mathrm{H}}[l]\boldsymbol{n}_s[l]. \end{aligned} \tag{14}$$

Based on (14), the target detection involves a binary hypothesis test problem given by [35]

$$
y_s[l] = \begin{cases} \mathcal{H}_l^0 : \boldsymbol{u}^{\mathrm{H}}[l] \sum\limits_{m\in\mathcal{M}} \alpha_m \varrho_m \boldsymbol{a}(\psi_m)\boldsymbol{a}^{\mathrm{H}}(\psi_m)\boldsymbol{x}[l] + \boldsymbol{u}^{\mathrm{H}}[l]\boldsymbol{n}_s[l], \\ \mathcal{H}_l^1 : \alpha_t \varrho_t \boldsymbol{u}^{\mathrm{H}}[l]\boldsymbol{a}(\phi_l)\boldsymbol{a}^{\mathrm{H}}(\phi_l)\boldsymbol{x}[l] + \boldsymbol{u}^{\mathrm{H}}[l] \sum\limits_{m\in\mathcal{M}} \alpha_m \varrho_m \boldsymbol{a}(\psi_m)\boldsymbol{a}^{\mathrm{H}}(\psi_m)\boldsymbol{x}[l] + \boldsymbol{u}^{\mathrm{H}}[l]\boldsymbol{n}_s[l], \end{cases} \tag{15}
$$

where $\mathcal{H}_l^0$ denotes the hypothesis that there is no target in sector $l$ while $\mathcal{H}_l^1$ represents the hypothesis that there is a target. The terms $\boldsymbol{u}^{\mathrm{H}}[l]\sum_{m\in\mathcal{M}}\alpha_m\varrho_m\boldsymbol{a}(\psi_m)\boldsymbol{a}^{\mathrm{H}}(\psi_m)\boldsymbol{x}[l]$ and $\boldsymbol{u}^{\mathrm{H}}[l]\boldsymbol{n}_s[l]$ denote interference and noise after receive combining, respectively. The optimal detector is given as follows [35]:

$$
Y = |y_s[l]|^2 \underset{H_0}{\overset{H_1}{\gtrless}} \delta, \tag{16}
$$

where $\delta$ is the decision threshold for a given false alarm probability $P_{\mathrm{FA}}$. The distribution of $Y$ is given by

$$
Y \sim \begin{cases} \varpi_0 \chi_2^2, & \mathcal{H}_0, \\ \varpi_1 \chi_2^2, & \mathcal{H}_1, \end{cases}
$$

where $\chi_2^2$ is the central chi-squared distribution with two DoFs [30]. Variables $\varpi_0$ and $\varpi_1$ are given by, respectively,

$$
\begin{aligned}
\varpi_0 =& \boldsymbol{u}^{\mathrm{H}}[l]\left(\sum_{m\in\mathcal{M}} \sigma_m^2 \varrho_m^2 \boldsymbol{A}_{\psi_m}\left(\sum_{k\in\mathcal{K}} \boldsymbol{w}_k[l]\boldsymbol{w}_k^{\mathrm{H}}[l] + \boldsymbol{R}[l]\right)\boldsymbol{A}_{\psi_m}^{\mathrm{H}}\right)\boldsymbol{u}[l] + \sigma_s^2\boldsymbol{u}^{\mathrm{H}}[l]\boldsymbol{u}[l], \\
\varpi_1 =& \sigma_t^2\varrho_t^2\boldsymbol{u}^{\mathrm{H}}[l]\boldsymbol{A}_{\phi_l}\left(\sum_{k\in\mathcal{K}} \boldsymbol{w}_k[l]\boldsymbol{w}_k^{\mathrm{H}}[l] + \boldsymbol{R}[l]\right)\boldsymbol{A}_{\phi_l}^{\mathrm{H}}\boldsymbol{u}[l] \\
&+ \boldsymbol{u}^{\mathrm{H}}[l]\left(\sum_{m\in\mathcal{M}} \sigma_m^2 \varrho_m^2 \boldsymbol{A}_{\psi_m}\left(\sum_{k\in\mathcal{K}} \boldsymbol{w}_k[l]\boldsymbol{w}_k^{\mathrm{H}}[l] + \boldsymbol{R}[l]\right)\boldsymbol{A}_{\psi_m}^{\mathrm{H}}\right)\boldsymbol{u}[l] + \sigma_s^2\boldsymbol{u}^{\mathrm{H}}[l]\boldsymbol{u}[l],
\end{aligned} \tag{17}
$$

where $\boldsymbol{A}_{\phi_l} \triangleq \boldsymbol{a}(\phi_l)\boldsymbol{a}^{\mathrm{H}}(\phi_l)$ and $\boldsymbol{A}_{\psi_m} \triangleq \boldsymbol{a}(\psi_m)\boldsymbol{a}^{\mathrm{H}}(\psi_m)$. Accordingly, the false alarm probability $P_{\mathrm{FA}}$ and detection probability $P_{\mathrm{D}}$ is given by, respectively,

$$
\begin{aligned}
P_{\mathrm{FA}} &= \Pr(Y > \delta \mid \mathcal{H}_0) = 1 - \mathcal{F}_{\chi_2^2}\left(\frac{\delta}{\varpi_0}\right), \\
P_{\mathrm{D}} &= \Pr(Y > \delta \mid \mathcal{H}_1) = 1 - \mathcal{F}_{\chi_2^2}\left(\frac{\delta}{\varpi_1}\right),
\end{aligned} \tag{18}
$$

where $\mathcal{F}_{\chi_2^2}(\cdot)$ is the cumulative distribution function of the central chi-squared distribution with two DoFs. For a given $P_{\mathrm{FA}}$, the detection probability $P_{\mathrm{D}}$ is given by

$$
P_{\mathrm{D}} = 1 - \mathcal{F}_{\chi_2^2}\left(\frac{\varpi_0}{\varpi_1}\mathcal{F}_{\chi_2^2}^{-1}(1 - P_{\mathrm{FA}})\right), \tag{19}
$$

where $\mathcal{F}_{\chi_2^2}^{-1}(\cdot)$ is the inverse function of $\mathcal{F}_{\chi_2^2}(\cdot)$. Note that $P_{\mathrm{D}}$ is a monotonically increasing function with respect to $\frac{\varpi_1}{\varpi_0}$ and $\frac{\varpi_1}{\varpi_0}$ is given by

$$
\begin{aligned}
\frac{\varpi_1}{\varpi_0} &= \frac{\sigma_t^2\varrho_t^2\boldsymbol{u}^{\mathrm{H}}[l]\boldsymbol{A}_{\phi_l}\left(\sum_{k\in\mathcal{K}}\boldsymbol{w}_k[l]\boldsymbol{w}_k^{\mathrm{H}}[l] + \boldsymbol{R}[l]\right)\boldsymbol{A}_{\phi_l}^{\mathrm{H}}\boldsymbol{u}[l]}{\boldsymbol{u}^{\mathrm{H}}[l]\left(\sum_{m\in\mathcal{M}}\sigma_m^2\varrho_m^2\boldsymbol{A}_{\psi_m}\left(\sum_{k\in\mathcal{K}}\boldsymbol{w}_k[l]\boldsymbol{w}_k^{\mathrm{H}}[l] + \boldsymbol{R}[l]\right)\boldsymbol{A}_{\psi_m}^{\mathrm{H}}\right)\boldsymbol{u}[l] + \sigma_s^2\boldsymbol{u}^{\mathrm{H}}[l]\boldsymbol{u}[l]} + 1 \\
&\triangleq \gamma_s[l] + 1,
\end{aligned} \tag{20}
$$

where $\gamma_s[l] \triangleq \frac{\sigma_t^2\varrho_t^2\boldsymbol{u}^{\mathrm{H}}[l]\boldsymbol{A}_{\phi_l}(\sum_{k\in\mathcal{K}}\boldsymbol{w}_k[l]\boldsymbol{w}_k^{\mathrm{H}}[l]+\boldsymbol{R}[l])\boldsymbol{A}_{\phi_l}^{\mathrm{H}}\boldsymbol{u}[l]}{\boldsymbol{u}^{\mathrm{H}}[l](\sum_{m\in\mathcal{M}}\sigma_m^2\varrho_m^2\boldsymbol{A}_{\psi_m}(\sum_{k\in\mathcal{K}}\boldsymbol{w}_k[l]\boldsymbol{w}_k^{\mathrm{H}}[l]+\boldsymbol{R}[l])\boldsymbol{A}_{\psi_m}^{\mathrm{H}})\boldsymbol{u}[l]+\sigma_s^2\boldsymbol{u}^{\mathrm{H}}[l]\boldsymbol{u}[l]}$. Hence, one can impose restrictions on $\gamma_s[l]$ to satisfy the required detection probability [30,36].

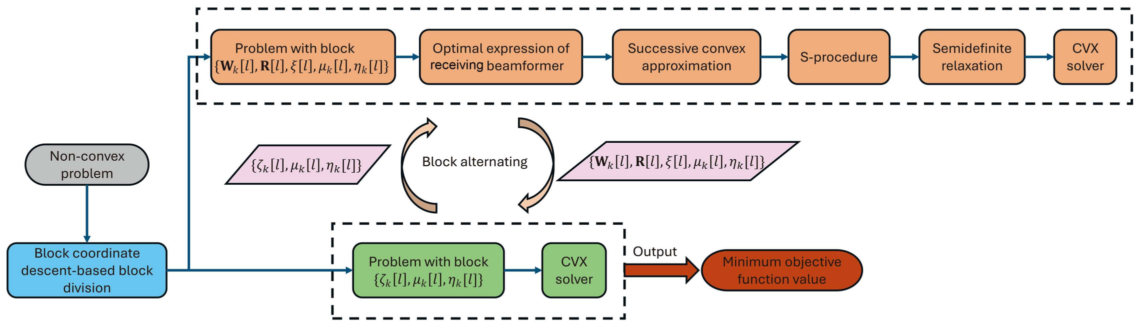


**Figure 2** (Color online) Key steps of the proposed optimization framework.

### 3.2 Problem formulation

In this paper, we aim to maximize the average sum rate while restricting the beampattern matching error and ensuring a desired detection probability by jointly optimizing the information beamforming $\boldsymbol{w}_k[l]$, radar covariance matrix $\boldsymbol{R}[l]$, receive beamformer $\boldsymbol{u}[l]$, and beampattern scaling factor $\xi[l]$ for all sectors. The corresponding optimization problem is formulated as follows:

$$\begin{aligned}
\underset{\substack{\boldsymbol{w}_k[l],\boldsymbol{R}[l],\\ \boldsymbol{u}[l],\xi[l]}}{\operatorname{maximize}} \quad & \min_{\Delta\boldsymbol{h}_k\in\Omega_k} \frac{1}{L}\sum_{l\in\mathcal{L}}\sum_{k\in\mathcal{K}} R_k[l] \\
\text{s.t.} \quad & \text{C1: } \mathcal{E}_l\left(\{\boldsymbol{w}_k[l]\}, \boldsymbol{R}[l], \xi[l]\right) \leqslant \epsilon_1,\ \forall l, \\
& \text{C2: } \gamma_s[l] \geqslant \epsilon_2,\ \forall l, \\
& \text{C3: } \sum_{k\in\mathcal{K}} \|\boldsymbol{w}_k[l]\|_2^2 + \operatorname{Tr}(\boldsymbol{R}[l]) \leqslant P_{\max}, \forall l,
\end{aligned} \tag{21}$$

where constraint C1 restricts the beampattern matching error of each sector to be smaller than a predefined threshold $\epsilon_1$ for a given desired resolution. Constraint C2 ensures the detection probability by imposing restrictions on $\gamma_s[l]$ to be larger than a pre-determined threshold $\epsilon_2$. Constraint C3 limits the transmit power of each sector from exceeding the maximum available power at BS, specified by $P_{\max}$.

Note that the problem in (21) is non-convex and difficult to solve. Specifically, the non-convexity originates from the variable coupling between $\boldsymbol{u}[l]$ and $\boldsymbol{w}_k[l]$ in constraint C2. Furthermore, the objective function involves complicated fractional expressions, and the continuous uncertainty set in the objective function leads to a semi-infinite programming problem with infinitely many constraints [37].

**Remark 2.** In this work, we aim to maximize the sum rate of the system without considering the quality of service (QoS) requirement of each user. Nevertheless, the proposed method can be adjusted to guarantee the communication QoS during the scanning period. Specifically, when performing detection for the $l$-th sector, we can simultaneously serve communication users in the same sector by the DFRC signals. For users in other sectors, we can generate additional information beams to guarantee their communication QoS. In the sensing receiver, the received signals due to the additional information beam can be separated from the desired echoes based on their unique angle-of-arrival (AoA).

## 4 BCD-based optimization

In this section, we develop a framework to handle problem (21) in polynomial time complexity with guaranteed convergence. Specifically, we handle the coupled variables in constraint C2 by finding the optimal expression for $\boldsymbol{u}[l]$. Then, constraint C2 is tackled by employing SCA. Furthermore, by introducing new variables and constraints, we transform the objective function into a more tractable form. Finally, we solve the problem by exploiting the BCD approach. The key steps of the proposed optimization framework are presented in Figure 2.

### 4.1 Problem reformulation

First, we define a new optimization variable $\boldsymbol{W}_k[l] \triangleq \boldsymbol{w}_k[l]\boldsymbol{w}_k^{\mathrm{H}}[l]$. This results in a new rank-one constraint C4: $\operatorname{Rank}(\boldsymbol{W}_k[l]) \leqslant 1, \forall k, \forall l$, which is imposed to ensure that $\boldsymbol{w}_k$ can be recovered from the optimized

$\boldsymbol{W}_k$. Accordingly, constraints C1 and C3 are reformulated equivalently as, respectively,

$$\begin{aligned}&\text{C1: } \sum_{i\in\mathcal{I}}\left|\xi[l]P_l(\theta_i)-\boldsymbol{a}^{\mathrm{H}}(\theta_i)\left(\sum_{k\in\mathcal{K}}\boldsymbol{W}_k[l]+\boldsymbol{R}[l]\right)\boldsymbol{a}(\theta_i)\right|^2\leqslant\epsilon_1,\ \forall l,\\&\text{C3: } \sum_{k\in\mathcal{K}}\mathrm{Tr}(\boldsymbol{W}_k[l])+\mathrm{Tr}(\boldsymbol{R}[l])\leqslant P_{\max},\ \forall l.\end{aligned}\tag{22}$$

We note that constraints C1 and C3 are both convex with respect to all optimization variables. Then, the optimization problem in (21) is transformed into

$$\begin{aligned}\underset{\substack{\boldsymbol{W}_k[l],\boldsymbol{R}[l],\\\boldsymbol{u}[l],\xi[l]}}{\text{maximize}}\quad&\min_{\Delta\boldsymbol{h}_k\in\Omega_k}\ \frac{1}{L}\sum_{l\in\mathcal{L}}\sum_{k\in\mathcal{K}}\log_2\left(1+\frac{\boldsymbol{h}_k^{\mathrm{H}}\boldsymbol{W}_k[l]\boldsymbol{h}_k}{\sum_{k'\in\mathcal{K}\setminus\{k\}}\boldsymbol{h}_k^{\mathrm{H}}\boldsymbol{W}_{k'}[l]\boldsymbol{h}_k+\boldsymbol{h}_k^{\mathrm{H}}\boldsymbol{R}[l]\boldsymbol{h}_k+\sigma_k^2}\right)\\\text{s.t.}\quad&\text{C1},\text{C3},\text{C4: Rank}(\boldsymbol{W}_k[l])\leqslant 1,\ \forall k,\ \forall l,\\&\text{C2: }\gamma_s[l]=\frac{\sigma_t^2\varrho_t^2\boldsymbol{u}^{\mathrm{H}}[l]\boldsymbol{A}_{\phi_l}\left(\sum_{k\in\mathcal{K}}\boldsymbol{W}_k[l]+\boldsymbol{R}[l]\right)\boldsymbol{A}_{\phi_l}^{\mathrm{H}}\boldsymbol{u}[l]}{\boldsymbol{u}^{\mathrm{H}}[l]\boldsymbol{F}[l]\boldsymbol{u}[l]}\geqslant\epsilon_2,\ \forall l,\end{aligned}\tag{23}$$

where $\boldsymbol{F}[l]$ is defined as $\boldsymbol{F}[l]=\sum_{m\in\mathcal{M}}\sigma_m^2\varrho_m^2\boldsymbol{A}_{\psi_m}\left(\sum_{k\in\mathcal{K}}\boldsymbol{W}_k[l]+\boldsymbol{R}[l]\right)\boldsymbol{A}_{\psi_m}^{\mathrm{H}}+\sigma_s^2\boldsymbol{I}$ for notational simplicity.

### 4.2 SCA-based method for handling non-convex constraint C2

The detection constraint C2 is intractable due to the coupling between optimization variables $\boldsymbol{u}[l]$ and $\boldsymbol{W}_k[l]$. However, we note that the receive beamformer $\boldsymbol{u}[l]$ only exists in constraint C2, and hence, the optimal $\boldsymbol{u}[l]$ should maximize $\gamma_s[l]$, which leads to the following problem [38]:

$$\underset{\boldsymbol{u}[l]}{\text{maximize}}\ \ \frac{\sigma_t^2\varrho_t^2\boldsymbol{u}^{\mathrm{H}}[l]\boldsymbol{A}_{\phi_l}\left(\sum_{k\in\mathcal{K}}\boldsymbol{W}_k[l]+\boldsymbol{R}[l]\right)\boldsymbol{A}_{\phi_l}^{\mathrm{H}}\boldsymbol{u}[l]}{\boldsymbol{u}^{\mathrm{H}}[l]\boldsymbol{F}[l]\boldsymbol{u}[l]}.\tag{24}$$

We note that the objective function can be further rewritten as

$$\frac{\sigma_t^2\varrho_t^2\boldsymbol{u}^{\mathrm{H}}[l]\boldsymbol{A}_{\phi_l}\left(\sum_{k\in\mathcal{K}}\boldsymbol{W}_k[l]+\boldsymbol{R}[l]\right)\boldsymbol{A}_{\phi_l}^{\mathrm{H}}\boldsymbol{u}[l]}{\boldsymbol{u}^{\mathrm{H}}[l]\boldsymbol{F}[l]\boldsymbol{u}[l]}=\frac{\sigma_t^2\varrho_t^2\boldsymbol{a}^{\mathrm{H}}(\phi_l)\left(\sum_{k\in\mathcal{K}}\boldsymbol{W}_k[l]+\boldsymbol{R}[l]\right)\boldsymbol{a}(\phi_l)\left|\boldsymbol{u}^{\mathrm{H}}[l]\boldsymbol{a}(\phi_l)\right|^2}{\boldsymbol{u}^{\mathrm{H}}[l]\boldsymbol{F}[l]\boldsymbol{u}[l]}.\tag{25}$$

Then, the optimization problem in (24) can be recast as

$$\underset{\boldsymbol{u}[l]}{\text{maximize}}\ \ \frac{\left|\boldsymbol{u}^{\mathrm{H}}[l]\boldsymbol{a}(\phi_l)\right|^2}{\boldsymbol{u}^{\mathrm{H}}[l]\boldsymbol{F}[l]\boldsymbol{u}[l]}.\tag{26}$$

The optimal solution to problem (26) is given by

$$\boldsymbol{u}^*[l]=\frac{\boldsymbol{F}^{-1}[l]\boldsymbol{a}(\phi_l)}{\boldsymbol{a}^{\mathrm{H}}(\phi_l)\boldsymbol{F}^{-1}[l]\boldsymbol{a}(\phi_l)}.\tag{27}$$

The detailed derivations are given in Appendix A. By substituting $\boldsymbol{u}^*[l]$ into constraint C2, we have

$$\overline{\text{C2}}\text{: } \sigma_t^2\varrho_t^2\boldsymbol{a}^{\mathrm{H}}(\phi_l)\left(\sum_{k\in\mathcal{K}}\boldsymbol{W}_k[l]+\boldsymbol{R}[l]\right)\boldsymbol{a}(\phi_l)\boldsymbol{a}^{\mathrm{H}}(\phi_l)\boldsymbol{F}^{-1}[l]\boldsymbol{a}(\phi_l)\geqslant\epsilon_2,\ \forall l.\tag{28}$$

Further, after some basic mathematical operations, constraint $\overline{\text{C2}}$ can be equivalently transformed into

$$\overline{\text{C2}}\text{: } \frac{\epsilon_2}{\sigma_t^2\varrho_t^2}\left(\boldsymbol{a}^{\mathrm{H}}(\phi_l)\left(\sum_{k\in\mathcal{K}}\boldsymbol{W}_k[l]+\boldsymbol{R}[l]\right)\boldsymbol{a}(\phi_l)\right)^{-1}-\boldsymbol{a}^{\mathrm{H}}(\phi_l)\boldsymbol{F}^{-1}[l]\boldsymbol{a}(\phi_l)\leqslant 0,\ \forall l.\tag{29}$$

We note that both $(\boldsymbol{a}^{\mathrm{H}}(\phi_l)(\sum_{k\in\mathcal{K}}\boldsymbol{W}_k[l]+\boldsymbol{R}[l])\boldsymbol{a}(\phi_l))^{-1}$ and $\boldsymbol{a}^{\mathrm{H}}(\phi_l)\boldsymbol{F}^{-1}[l]\boldsymbol{a}(\phi_l)$ in constraint $\overline{\mathrm{C2}}$ are convex with respect to all optimization variables. As a result, constraint $\overline{\mathrm{C2}}$ is in the canonical form of the difference of convex functions, which can be efficiently tackled by employing the SCA method. Specifically, we construct a global lower-bound based on the first-order Taylor approximation of the term $f(\boldsymbol{W}_k[l],\boldsymbol{R}[l])\overset{\triangle}{=}\boldsymbol{a}^{\mathrm{H}}(\phi_l)\boldsymbol{F}^{-1}[l]\boldsymbol{a}(\phi_l)$. In the $t$-th iteration of SCA, $f(\boldsymbol{W}_k[l],\boldsymbol{R}[l])$ is approximated at a feasible point $(\boldsymbol{W}_k^{(t-1)}[l],\boldsymbol{R}^{(t-1)}[l])$ as follows:

$$\begin{aligned}f(\boldsymbol{W}_k[l],\boldsymbol{R}[l])\geqslant& f(\boldsymbol{W}_k^{(t-1)}[l],\boldsymbol{R}^{(t-1)}[l])+\mathrm{Tr}\left(\nabla_{\boldsymbol{R}}^{\mathrm{H}}f(\boldsymbol{W}_k^{(t-1)}[l],\boldsymbol{R}^{(t-1)}[l])\left(\boldsymbol{R}[l]-\boldsymbol{R}^{(t-1)}[l]\right)\right)\\&+\sum_{k\in\mathcal{K}}\mathrm{Tr}\left(\nabla_{\boldsymbol{W}_k}^{\mathrm{H}}f(\boldsymbol{W}_k^{(t-1)}[l],\boldsymbol{R}^{(t-1)}[l])\left(\boldsymbol{W}_k[l]-\boldsymbol{W}_k^{(t-1)}[l]\right)\right)\\&\overset{\triangle}{=}\overline{f}^{(t)}(\boldsymbol{W}_k[l],\boldsymbol{R}[l]),\end{aligned}\tag{30}$$

where

$$\begin{aligned}\nabla_{\boldsymbol{R}[l]}f(\boldsymbol{W}_k[l],\boldsymbol{R}[l])&=-\sum_{m\in\mathcal{M}}\sigma_m^2\varrho_m^2\boldsymbol{A}_{\psi_m}^{\mathrm{H}}\boldsymbol{F}^{-1}[l]\boldsymbol{A}_{\phi_l}\boldsymbol{F}^{-1}[l]\boldsymbol{A}_{\psi_m}^{\mathrm{H}},\\\nabla_{\boldsymbol{W}_k[l]}f(\boldsymbol{W}_k[l],\boldsymbol{R}[l])&=-\sum_{m\in\mathcal{M}}\sigma_m^2\varrho_m^2\boldsymbol{A}_{\psi_m}^{\mathrm{H}}\boldsymbol{F}^{-1}[l]\boldsymbol{A}_{\phi_l}\boldsymbol{F}^{-1}[l]\boldsymbol{A}_{\psi_m}^{\mathrm{H}}.\end{aligned}\tag{31}$$

Here, $\boldsymbol{W}_k^{(t-1)}[l]$ and $\boldsymbol{R}^{(t-1)}[l]$ denote the optimization variables obtained in the $(t-1)$-th iteration of SCA. $\overline{f}^{(t)}(\boldsymbol{W}_k[l],\boldsymbol{R}[l])$ denotes the approximation of $f(\boldsymbol{W}_k[l],\boldsymbol{R}[l])$ in the $t$-th iteration of SCA. As a result, by applying SCA, constraint $\overline{\mathrm{C2}}$ in the $t$-th iteration of SCA algorithm is given by

$$\overline{\overline{\mathrm{C2}}}\text{: }\frac{\epsilon_2}{\sigma_t^2\varrho_t^2}\left(\boldsymbol{a}^{\mathrm{H}}(\phi_l)\left(\sum_{k\in\mathcal{K}}\boldsymbol{W}_k[l]+\boldsymbol{R}[l]\right)\boldsymbol{a}(\phi_l)\right)^{-1}-\overline{f}^{(t)}(\boldsymbol{W}_k[l],\boldsymbol{R}[l])\leqslant 0,\ \forall l.\tag{32}$$

Therefore, the optimization problem to be solved at the $t$-th iteration is given by

$$\begin{aligned}\underset{\substack{\boldsymbol{W}_k[l],\boldsymbol{R}[l],\\\xi[l]}}{\mathrm{maximize}}\quad&\min_{\Delta\boldsymbol{h}_k\in\Omega_k}\ \frac{1}{L}\sum_{l\in\mathcal{L}}\sum_{k\in\mathcal{K}}\log_2\left(1+\frac{\boldsymbol{h}_k^{\mathrm{H}}\boldsymbol{W}_k[l]\boldsymbol{h}_k}{\sum_{k'\in\mathcal{K}\setminus\{k\}}\boldsymbol{h}_k^{\mathrm{H}}\boldsymbol{W}_{k'}[l]\boldsymbol{h}_k+\boldsymbol{h}_k^{\mathrm{H}}\boldsymbol{R}[l]\boldsymbol{h}_k+\sigma_k^2}\right)\\\mathrm{s.t.}\quad&\mathrm{C1},\overline{\overline{\mathrm{C2}}},\mathrm{C3},\mathrm{C4}.\end{aligned}\tag{33}$$

### 4.3 Handling the non-convex objective function

The objective function of (21) involves non-convex fractional expression and semi-infinite programming. To tackle these obstacles, we first simplify the expression by introducing auxiliary variables $\mu_k[l],k\in\mathcal{K},l\in\mathcal{L}$, and the following constraint:

$$\mathrm{C5}\text{: }\mu_k[l]\leqslant\min_{\Delta\boldsymbol{h}_k\in\Omega_k}\log_2\left(1+\frac{\boldsymbol{h}_k^{\mathrm{H}}\boldsymbol{W}_k[l]\boldsymbol{h}_k}{\sum_{k'\in\mathcal{K}\setminus\{k\}}\boldsymbol{h}_k^{\mathrm{H}}\boldsymbol{W}_{k'}[l]\boldsymbol{h}_k+\boldsymbol{h}_k^{\mathrm{H}}\boldsymbol{R}[l]\boldsymbol{h}_k+\sigma_k^2}\right),\forall k,\forall l.\tag{34}$$

The objective function is accordingly substituted by $\sum_{l\in\mathcal{L}}\sum_{k\in\mathcal{K}}\mu_k[l]$. To handle constraint C5, we introduce variables $\zeta_k[l],k\in\mathcal{K},l\in\mathcal{L}$. Constraint C5 is then equivalently transformed into the following two constraints:

$$\begin{aligned}&\mathrm{C5a}\text{: }\mu_k[l]\leqslant\log_2(1+\zeta_k[l]),\ \forall k,\ \forall l,\\&\mathrm{C5b}\text{: }\zeta_k[l]\leqslant\min_{\Delta\boldsymbol{h}_k\in\Omega_k}\frac{\boldsymbol{h}_k^{\mathrm{H}}\boldsymbol{W}_k[l]\boldsymbol{h}_k}{\sum_{k'\in\mathcal{K}\setminus\{k\}}\boldsymbol{h}_k^{\mathrm{H}}\boldsymbol{W}_{k'}[l]\boldsymbol{h}_k+\boldsymbol{h}_k^{\mathrm{H}}\boldsymbol{R}[l]\boldsymbol{h}_k+\sigma_k^2},\ \forall k,\ \forall l,\end{aligned}\tag{35}$$

where constraint C5a is convex with respect to all optimization variables. Yet, constraint C5b is non-convex and intractable due to the complicated fractional expression and the continuous uncertainty set. To circumvent this difficulty, we first rewrite the fractional expression in C5b as follows:

$$\overline{\mathrm{C5b}}\text{: }\boldsymbol{h}_k^{\mathrm{H}}\boldsymbol{W}_k[l]\boldsymbol{h}_k-\zeta_k[l]\sum_{k'\in\mathcal{K}\setminus\{k\}}\boldsymbol{h}_k^{\mathrm{H}}\boldsymbol{W}_{k'}[l]\boldsymbol{h}_k-\zeta_k[l]\boldsymbol{h}_k^{\mathrm{H}}\boldsymbol{R}[l]\boldsymbol{h}_k-\zeta_k[l]\sigma_k^2\geqslant 0,\ \forall k,\ \forall l,\ \Delta\boldsymbol{h}_k\in\Omega_k.\tag{36}$$

Next, we deal with the semi-infinite programming problem caused by $\Delta\boldsymbol{h}_k \in \Omega_k$ by exploiting the following lemma.

**Lemma 1** (S-Procedure Lemma [39])**.** Define two functions $f_i(\boldsymbol{t}) : \mathbb{C}^N \to \mathbb{R}$, $i \in \{1,2\}$ as

$$f_i(\boldsymbol{t}) = \boldsymbol{t}^{\mathrm{H}}\boldsymbol{A}_i\boldsymbol{t} + 2\Re\left\{\boldsymbol{b}_i^{\mathrm{H}}\boldsymbol{t}\right\} + c_i, \tag{37}$$

where $\boldsymbol{A}_i \in \mathbb{H}^N$, $\boldsymbol{b}_i \in \mathbb{C}^N$, and $c_i \in \mathbb{R}$. Then, the implication $f_1(\boldsymbol{t}) \leqslant 0 \Rightarrow f_2(\boldsymbol{t}) \leqslant 0$ holds if and only if there exists a variable $\kappa \geqslant 0$ such that

$$\kappa \begin{bmatrix} \boldsymbol{A}_1 & \boldsymbol{b}_1 \\ \boldsymbol{b}_1^{\mathrm{H}} & c_1 \end{bmatrix} - \begin{bmatrix} \boldsymbol{A}_2 & \boldsymbol{b}_2 \\ \boldsymbol{b}_2^{\mathrm{H}} & c_2 \end{bmatrix} \succeq \boldsymbol{0}. \tag{38}$$

We first reformulate constraint $\overline{\mathrm{C5b}}$ by substituting (4) in $\overline{\mathrm{C5b}}$ as follows:

$$\begin{aligned}\overline{\mathrm{C5b}}\text{: } & \Delta\boldsymbol{h}_k^{\mathrm{H}}\left(\zeta_k[l]\left(\sum_{k'\in\mathcal{K}\setminus\{k\}}\boldsymbol{W}_{k'}[l] + \boldsymbol{R}[l]\right) - \boldsymbol{W}_k[l]\right)\Delta\boldsymbol{h}_k \\ & + 2\Re\left\{\overline{\boldsymbol{h}}_k^{\mathrm{H}}\left(\zeta_k[l]\left(\sum_{k'\in\mathcal{K}\setminus\{k\}}\boldsymbol{W}_{k'}[l] + \boldsymbol{R}[l]\right) - \boldsymbol{W}_k[l]\right)\Delta\boldsymbol{h}_k\right\} \\ & + \overline{\boldsymbol{h}}_k^{\mathrm{H}}\left(\zeta_k[l]\left(\sum_{k'\in\mathcal{K}\setminus\{k\}}\boldsymbol{W}_{k'}[l] + \boldsymbol{R}[l]\right) - \boldsymbol{W}_k[l]\right)\overline{\boldsymbol{h}}_k + \zeta_k[l]\sigma_k^2 \leqslant 0,\ \forall k,\ \forall l,\ \Delta\boldsymbol{h}_k \in \Omega_k.\end{aligned} \tag{39}$$

According to Lemma 1, the implication $\Delta\boldsymbol{h}_k^{\mathrm{H}}\Delta\boldsymbol{h}_k - \beta_k^2 \leqslant 0 \Rightarrow \overline{\mathrm{C5b}}$ holds if and only if there exists $\eta_k[l] \geqslant 0$, $k \in \mathcal{K}$, $l \in \mathcal{L}$, satisfying the following linear matrix inequality (LMI) constraint:

$$\overline{\overline{\mathrm{C5b}}}\text{: } \eta_k[l]\begin{bmatrix} \boldsymbol{I}_N & \boldsymbol{0} \\ \boldsymbol{0} & -\beta_k^2 \end{bmatrix} - \begin{bmatrix} \widetilde{\boldsymbol{W}}_k[l] & \widetilde{\boldsymbol{W}}_k^{\mathrm{H}}[l]\overline{\boldsymbol{h}}_k \\ \overline{\boldsymbol{h}}_k^{\mathrm{H}}\widetilde{\boldsymbol{W}}_k[l] & \overline{\boldsymbol{h}}_k^{\mathrm{H}}\widetilde{\boldsymbol{W}}_k[l]\overline{\boldsymbol{h}}_k + \zeta_k[l]\sigma_k^2 \end{bmatrix} \succeq \boldsymbol{0},\ \forall k,\ \forall l, \tag{40}$$

where $\widetilde{\boldsymbol{W}}_k[l] \triangleq \zeta_k[l](\sum_{k'\in\mathcal{K}\setminus\{k\}}\boldsymbol{W}_{k'}[l] + \boldsymbol{R}[l]) - \boldsymbol{W}_k[l]$. Furthermore, constraint $\overline{\overline{\mathrm{C5b}}}$ can be simplified as

$$\overline{\overline{\mathrm{C5b}}}\text{: } \begin{bmatrix} \eta_k[l]\boldsymbol{I}_N & \boldsymbol{0} \\ \boldsymbol{0} & -\eta_k[l]\beta_k^2 - \zeta_k[l]\sigma_k^2 \end{bmatrix} - \boldsymbol{U}_k^{\mathrm{H}}\widetilde{\boldsymbol{W}}_k[l]\boldsymbol{U}_k \succeq \boldsymbol{0},\ \forall k,\ \forall l, \tag{41}$$

where $\boldsymbol{U}_k \triangleq [\boldsymbol{I}_N\ \overline{\boldsymbol{h}}_k]$. As a result, the original optimization problem is transformed into

$$\begin{aligned} \underset{\substack{\boldsymbol{W}_k[l],\boldsymbol{R}[l],\\ \xi[l],\mu_k[l],\\ \zeta_k[l],\eta_k[l]}}{\text{maximize}}\ & \frac{1}{L}\sum_{l\in\mathcal{L}}\sum_{k\in\mathcal{K}}\mu_k[l] \\ \text{s.t.}\ & \mathrm{C1}, \overline{\overline{\mathrm{C2}}}, \mathrm{C3}, \mathrm{C4}, \mathrm{C5a}, \overline{\overline{\mathrm{C5b}}}. \end{aligned} \tag{42}$$

### 4.4 BCD-based algorithm

We note that the optimization variables $\zeta_k[l]$ are coupled with $\boldsymbol{W}_k[l]$ and $\boldsymbol{R}[l]$ in constraint $\overline{\overline{\mathrm{C5b}}}$. To overcome this difficulty, we propose to employ the BCD method. Specifically, the optimization variables are partitioned into two blocks, i.e., $\{\boldsymbol{W}_k[l], \boldsymbol{R}[l], \xi[l], \mu_k[l], \eta_k[l]\}$ and $\{\zeta_k[l], \mu_k[l], \eta_k[l]\}$. Note that the variables $\mu_k$ and $\eta_k$ are included in both blocks because they are not coupled with other variables and the two sub-problems are convex with respect to $\mu_k$ and $\eta_k$. As a result, solving the sub-problems yields a jointly optimal solution for $\mu_k$, $\eta_k$, and other variables in each block. This approach results in a larger feasible solution space for each sub-problem compared to the configuration where $\mu_k$ and $\eta_k$ are optimized in separable blocks. The optimization problem with block $\{\boldsymbol{W}_k[l], \boldsymbol{R}[l], \xi[l], \mu_k[l], \eta_k[l]\}$ is given by

$$\underset{\substack{\boldsymbol{W}_k[l],\boldsymbol{R}[l],\\ \xi[l],\mu_k[l],\eta_k[l]}}{\text{maximize}}\ \frac{1}{L}\sum_{l\in\mathcal{L}}\sum_{k\in\mathcal{K}}\mu_k[l]$$

**Algorithm 1** SCA-based algorithm for handling the problem with block $\{\boldsymbol{W}_k[l], \boldsymbol{R}[l], \xi[l], \mu_k[l], \eta_k[l]\}$.

1: Set iteration index $t = 1$ and convergence tolerance factor $0 < \varepsilon_1 \ll 1$ and generate the initial values $\boldsymbol{W}_k^{(0)}$ and $\boldsymbol{R}^{(0)}$.
2: **repeat**
3: Solve problem (44) for given $\boldsymbol{W}_k^{(t-1)}$ and $\boldsymbol{R}^{(t-1)}$;
4: Update $\boldsymbol{W}_k^{(t)}$, $\boldsymbol{R}^{(t)}$, $\xi^{(t)}[l]$, $\mu_k^{(t)}[l]$, and $\eta_k^{(t)}[l]$;
5: Set $t = t + 1$;
6: **until** $\frac{|g_1^{(t)} - g_1^{(t-1)}|}{g_1^{(t-1)}} \leqslant \varepsilon_1$.

**Algorithm 2** BCD-based algorithm.

1: Set iteration index $r = 0$ and convergence tolerance factor $0 < \varepsilon_2 \ll 1$ and initialize $\zeta_k^{(0)}[l]$.
2: **repeat**
3: Solve problem (44) for given $\zeta_k^{(r)}[l]$ by applying Algorithm 1;
4: Update $\boldsymbol{W}_k^{(r+1)}$, $\boldsymbol{R}^{(r+1)}$, and $\xi^{(r+1)}[l]$;
5: Solve problem (45) for given $\boldsymbol{W}_k^{(r+1)}$ and $\boldsymbol{R}^{(r+1)}$;
6: Update $\zeta_k^{(r+1)}[l]$, $\mu_k^{(r+1)}[l]$, and $\eta_k^{(r+1)}[l]$;
7: Set $r = r + 1$;
8: **until** $\frac{|g_2^{(r)} - g_2^{(r-1)}|}{g_2^{(r-1)}} \leqslant \varepsilon_2$.

$$\text{s.t.} \quad \text{C1}, \overline{\overline{\text{C2}}}, \text{C3}, \text{C4}, \text{C5a}, \overline{\overline{\text{C5b}}}. \tag{43}$$

We note that the only non-convexity in (43) originates from the rank-one constraint C4. To tackle this obstacle, we employ semidefinite relaxation (SDR) to remove constraint C4. The relaxed version of (43) is a convex optimization problem, which can be efficiently solved by standard convex optimization solvers [40]. The tightness of the SDR is revealed by the following proposition.

**Proposition 1.** For any optimal solution to problem (43), one can always construct the equivalent optimal beamforming matrix $\boldsymbol{W}_k^*$ which satisfies the rank-one constraint C4, i.e., $\text{Rank}(\boldsymbol{W}_k^*) \leqslant 1$.

*Proof.* The proof follows the similar steps in [41, Appendix B] and is omitted here for brevity.

The relaxed optimization problem is given by

$$\begin{aligned}
&\underset{\substack{\boldsymbol{W}_k[l], \boldsymbol{R}[l], \\ \xi[l], \mu_k[l], \eta_k[l]}}{\text{maximize}} \quad \frac{1}{L} \sum_{l \in \mathcal{L}} \sum_{k \in \mathcal{K}} \mu_k[l] \\
&\quad \text{s.t.} \quad \text{C1}, \text{C3}, \text{C5a}, \overline{\overline{\text{C5b}}}, \\
&\quad\quad \overline{\overline{\text{C2}}}\text{:} \ \frac{\epsilon_2}{\sigma_t^2} \left( \boldsymbol{a}^{\mathrm{H}}(\phi_l) \left( \sum_{k \in \mathcal{K}} \boldsymbol{W}_k[l] + \boldsymbol{R}[l] \right) \boldsymbol{a}(\phi_l) \right)^{-1} - \overline{f}^{(t)}(\boldsymbol{W}_k[l], \boldsymbol{R}[l]) \leqslant 0.
\end{aligned} \tag{44}$$

The solution to the block $\{\boldsymbol{W}_k[l], \boldsymbol{R}[l], \xi[l], \mu_k[l], \eta_k[l]\}$ is obtained by iteratively solving the optimization problem (44), and the developed SCA algorithm is summarized in Algorithm 1, where $g_1^{(t)}$ denotes the objective function value of (44) in the $t$-th iteration of SCA.

Next, we solve the optimization problem associated with the block $\{\zeta_k[l], \mu_k[l], \eta_k[l]\}$, which is given by

$$\begin{aligned}
&\underset{\zeta_k[l], \mu_k[l], \eta_k[l]}{\text{maximize}} \quad \frac{1}{L} \sum_{l \in \mathcal{L}} \sum_{k \in \mathcal{K}} \mu_k[l] \\
&\quad \text{s.t.} \quad \text{C5a}, \overline{\overline{\text{C5b}}}.
\end{aligned} \tag{45}$$

We note that (45) is a convex optimization problem and can be solved optimally in polynomial time complexity. The overall BCD-based algorithm is summarized in Algorithm 2, where $g_2^{(r)}$ denotes the objective function value of (45) in the $r$-th iteration of BCD.

Some remarks on the proposed algorithms are as follows.

(i) Convergence. For Algorithm 1, the objective function $g_1^{(t)}$ is monotonically non-decreasing and thus is guaranteed to converge to a stationary solution in polynomial time complexity [42]. Moreover, due to the monotonicity of $g_1^{(t)}$ in Algorithm 1, the value of the objective function of the problem associated with block $\{\boldsymbol{W}_k[l], \boldsymbol{R}[l], \xi[l], \mu_k[l], \eta_k[l]\}$ is also non-decreasing in each iteration of Algorithm 2. Considering the fact that the optimization problem associated with block $\{\zeta_k[l], \mu_k[l], \eta_k[l]\}$ is convex, the objective function of (42) is non-decreasing in each iteration. Therefore, the BCD-based algorithm is guaranteed to converge to a stationary solution to the optimization problem in (21) in polynomial time complexity [43].

(ii) Complexity. We note that the optimization problem associated with the block $\{\zeta_k[l], \mu_k[l], \eta_k[l]\}$ involves only scalar optimization variables. In contrast, for the optimization problem associated with block $\{\boldsymbol{W}_k[l], \boldsymbol{R}[l], \xi[l], \mu_k[l], \eta_k[l]\}$, we have to deal with $L(K+1)$ $N$-dimensional positive semidefinite matrices. Hence, the computational complexity of the proposed BCD-based algorithm is dominated by solving the optimization problem in (44) [44]. According to [45, Theorem 3.12], the computational complexity for solving an SDP problem with $m$ SDP constraints consisting of $n$-dimentional positive semidefinite matrix is given by $\mathcal{O}(mn^3 + m^2n^2 + m^3)$. Hence, the computational complexity of each iteration of Algorithm 2 is given by $\mathcal{O}(\log_2(\frac{1}{\varepsilon_1})((K+3)LN^3 + (K+3)^2L^2N^2 + (K+3)^3L^3))$, where $\varepsilon_1$ is the convergence tolerance defined in Algorithm 1.

## 5 Numerical results

### 5.1 Simulation setup

In this subsection, we adopt simulation results to validate the effectiveness of the proposed algorithms. The considered system is shown in Figure 3. We consider a system with one BS and $K = 3$ users. The BS is equipped with a ULA, which consists of $N = 16$ antennas and is centered at the origin of the coordinate system parallel to the $x$-axis. The BS monitors the area starting from 67.5°. The number of sectors is determined by $L = \lceil \frac{45^\circ}{\Delta\theta} \rceil$. Unless otherwise specified, we adopt the parameters summarized in Table 1 [46–49].

For comparison purposes, we consider the following baseline schemes.

**Baseline scheme 1.** Baseline scheme 1 separately designs the detection and communication approaches. Specifically, the radar covariance matrix $\boldsymbol{R}[l]$ and receive beamformer $\boldsymbol{u}[l]$ are first designed to satisfy the requirements for beampattern matching constraint C1 and detection requirement C2 with the minimum power consumption, which is formulated as

$$\begin{aligned} \underset{\substack{\boldsymbol{R}[l],\boldsymbol{u}[l],\\ \xi[l]}}{\operatorname{minimize}} \quad & \operatorname{Tr}(\boldsymbol{R}[l]) \\ \text{s.t.} \quad & \text{C1}, \text{C2}. \end{aligned} \tag{46}$$

After satisfying the detection requirements, the system designs the information beamformer $\boldsymbol{w}_k[l]$ to maximize the sum rate of communication users with the remaining power.

**Baseline scheme 2.** Baseline scheme 2 controls the beamwidth by adjusting the number of activated antennas [21,23]. Specifically, the half-power beamwidth $\Delta\theta$ of the antenna array with $N$ antennas toward the direction $\phi_l$ can be approximated by

$$\Delta\theta = \frac{1.78}{N\sin(\phi_l)}. \tag{47}$$

Accordingly, the required beamwidth can be achieved by dynamically activating antennas, where the number of antennas for sector $l$ is determined by $\lceil \frac{1.78}{\Delta\theta \sin(\phi_l)} \rceil$. Furthermore, the beamforming vector is determined by the steering vector toward the direction of the user. Accordingly, the constraint $\overline{\overline{\text{C5b}}}$ can be written as

$$\widetilde{\text{C5b}}\text{: } (1+\zeta_k[l])\operatorname{Tr}(\boldsymbol{H}_k\boldsymbol{W}_k[l]) - \zeta_k[l]\left(\sum_{k\in\mathcal{K}}\operatorname{Tr}(\boldsymbol{H}_k\boldsymbol{W}_k[l]) + \operatorname{Tr}(\boldsymbol{H}_k\boldsymbol{R}[l])\right) - \zeta_k[l]\sigma_k^2 \geqslant 0, \forall k, \forall l, \tag{48}$$

where $\boldsymbol{H}_k \triangleq \boldsymbol{h}_k\boldsymbol{h}_k^{\mathrm{H}}$.

### 5.2 Convergence of the proposed algorithm

Figure 4 presents the convergence behavior of the proposed algorithm with two maximum power constraints for each sector $P_{\max}$. It can be observed that for two cases, the objective value achieved by

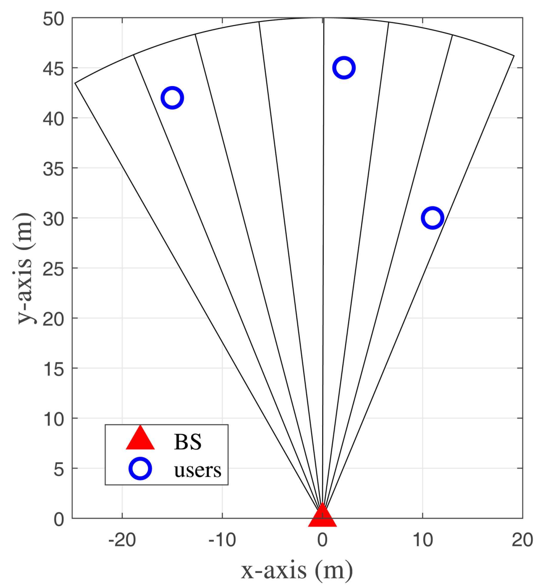


**Figure 3** (Color online) System setup of the system, which consists of $K = 3$ users, $L = 7$ sectors.

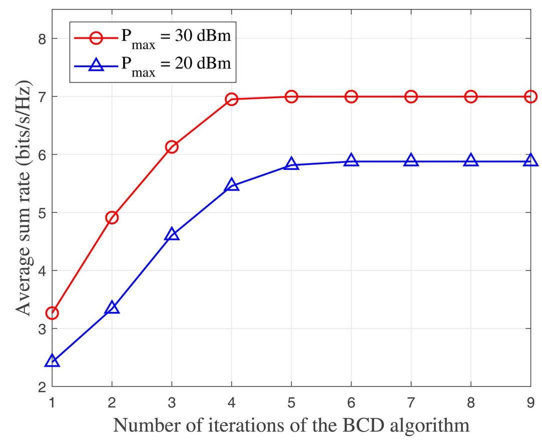


**Figure 4** (Color online) Convergence of the proposed BCD-based algorithm for different values of the maximum available powder (dBm) for each sector $P_{\max}$.

**Table 1** System simulation parameters.

| Symbol | Name | Value |
|---|---|---|
| $P_{\max}$ | Maximum power of each sector | 30 dBm |
| $f_c$ | System carrier frequency | 5 GHz [46] |
| $\sigma_k^2$ | Noise power at the $k$-th user | $-90$ dBm |
| $\sigma_s^2$ | Noise power at the BS | $-100$ dBm |
| $\sigma_t^2$ | Variance of RCS of the target | 0.1 |
| $\sigma_m^2$ | Variance of RCS of the clutters | 0.1 |
| $\varepsilon_1$, $\varepsilon_2$ | Error tolerance of Algorithms 1 and 2 | $10^{-3}$ |
| $\epsilon_1$ | Maximum tolerance of beampattern matching error | 0.1 [47] |
| $\epsilon_2$ | Minimum threshold for detection constraint | 15 dB [48] |
| $I$ | Number of sampled angles | 640 |
| $d$ | Detection distance | 50 m |
| $\Delta\theta$ | Required beamwidth of each sector | 0.12 rad |
| $\varsigma_s$ | pathloss exponent of sensing channel | 2 [49] |

the proposed algorithm monotonically increases and converges to a stationary solution. The algorithm with $P_{\max} = 30$ dBm converges to a higher objective value than the case of $P_{\max} = 20$ dBm. This is because the larger $P_{\max}$ expands the feasible region of the optimization problem, hence leading to a higher objective value.

### 5.3 Effect of resolution-aware beamwidth

In Figure 5, we investigate the effect of beamwidth $\Delta\theta$ with different resolution requirements. Note that the number of sectors changes with $\Delta\theta$. For a fair comparison, we set the same total power for different numbers of sectors. Specifically, the maximum available power for each sector is given by $P_{\max}^{(\Delta\theta_i)} = \frac{L}{L^{(\Delta\theta_i)}} P_{\max}$, where $L^{(\Delta\theta_i)}$ and $P_{\max}^{(\Delta\theta_i)}$ denote the number of sectors and the maximum available power for each sector with beamwidth $\Delta\theta_i$. As is shown in Figure 5, the average sum rate presents a step-like decreasing property. This is because the number of sectors changes with different sector beamwidth. In particular, the number of sectors $L$ is 7, 6 and 5 when $\Delta\theta$ falls in the regions $[0.12, 0.13]$, $[0.135, 0.155]$ and $\{0.16\}$, respectively. The average sum rate slightly decreases when $\Delta\theta$ increases in each interval with an unchanged number of sectors. Furthermore, the average sum rate shows a significant decline when $\Delta\theta$ increases with different numbers of sectors $L$, due to the reduced design DoFs.

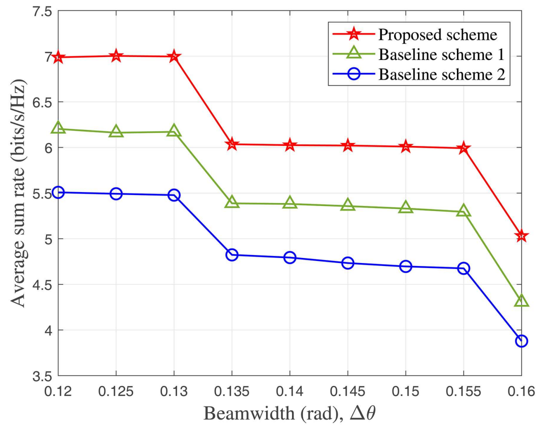


**Figure 5** (Color online) Average sum rate (bits/s/Hz) versus beamwidth (rad), $\Delta\theta$.

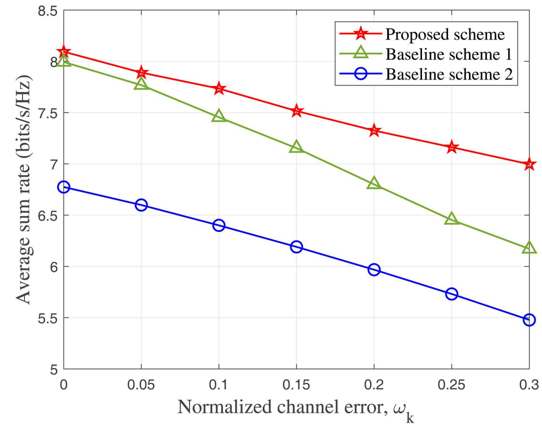


**Figure 6** (Color online) Average sum rate (bits/s/Hz) versus normalized channel error, $\omega_k$.

Moreover, it can be observed that the proposed scheme outperforms the two baseline schemes. Compared with baseline scheme 1, the performance improvement comes from the joint optimization of the radar covariance matrix, receive beamforming for sensing purposes, and information beamforming for communication purposes. The proposed scheme provides a flexible beamforming policy by utilizing part of information beamforming to satisfy the sensing requirements. Compared with baseline scheme 2, the proposed scheme benefits from the flexible beamforming capability without damaging the DoFs.

### 5.4 Effect of normalized channel error

Figure 6 investigates the effect of normalized channel error on the system average sum rate. For ease of presentation, we denote the normalized channel error as $\omega_k \triangleq \frac{\beta_k}{\|\boldsymbol{h}_k\|_2}$ [47]. As shown in Figure 6, the average sum rate decreases with $\omega_k$. This is because the beamforming policy becomes less flexible to satisfy the quality-of-service of users with larger CSI uncertainty. From the optimization perspective, larger $\omega_k$ makes the semi-infinite programming originating from the objective function of (21) more stringent and shrinks the feasible region, leading to performance degradation. Also, it can be observed that the proposed scheme outperforms the baseline schemes. The gap between the proposed scheme and baseline scheme 1 becomes larger as $\omega_k$ increases. This is because the proposed scheme benefits from a more flexible information beamformer design to handle imperfect CSI. Note that $\omega_k = 0$ corresponds to the case of no CSI error. The gap between the proposed scheme and the baseline scheme 2 in the case of $\omega_k = 0$ comes from two aspects. Firstly, the proposed scheme relies on the joint beamforming design to satisfy the beamwidth requirement without adjusting the number of antennas. Secondly, the optimized beamformer of the proposed scheme can exploit all available DoFs rather than being restricted to be the steering vector.

### 5.5 Effect of detection threshold

Figure 7 investigates the effect of the detection threshold, $\epsilon_2$ on the average sum rate. As can be observed, the proposed scheme only suffers slight performance loss for large $\epsilon_2$ and substantially outperforms the baseline schemes. The gap between the proposed scheme and the baseline scheme 1 increases significantly with $\epsilon_2$. This is because, for small $\epsilon_2$, the separately designed radar signal consumes a relatively small amount of energy, causing little effect on the sum rate maximization design. As $\epsilon_2$ increases, the remaining power for communication design in baseline scheme 1 decreases dramatically. Hence, the performance deterioration caused by the separate design becomes obvious and enlarges the gap. On the contrary, by exploiting the joint optimization of detection and communication, the proposed scheme is able to satisfy stringent detection requirements with little impact on communication performance.

### 5.6 Trade-off between sensing and communication performance

Figure 8 investigates the trade-off between sensing and communication. In particular, we illustrate the system sum rate under different thresholds for beampattern matching errors. As can be observed, the

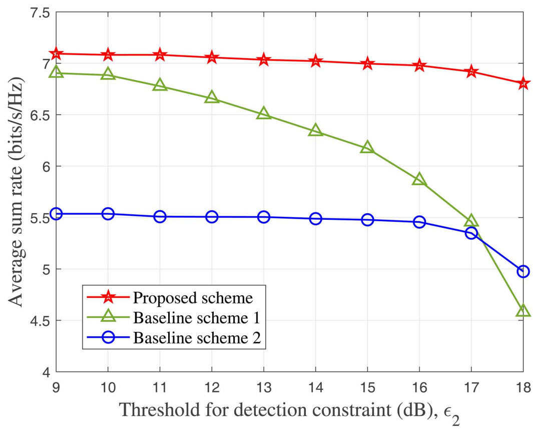


**Figure 7** (Color online) Average sum rate (bits/s/Hz) versus threshold for detection constraint (dB), $\epsilon_2$.

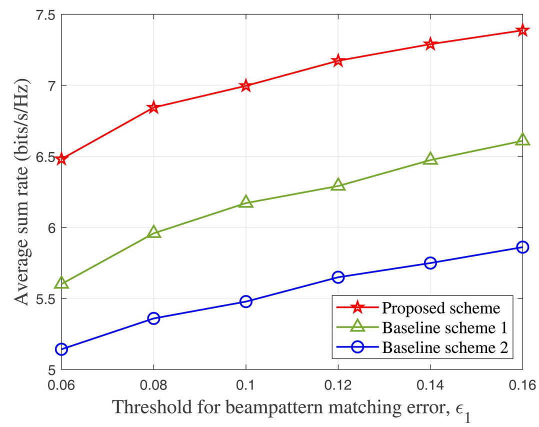


**Figure 8** (Color online) Average sum rate (bits/s/Hz) versus threshold for beampattern matching error, $\epsilon_1$.

average sum rate increases with $\epsilon_1$. By relaxing the beampattern restrictions, a more flexible beamforming strategy can be designed to achieve better communication performance, indicating the non-trivial tradeoff between sensing and communication services. Furthermore, the proposed scheme achieves the highest sum rate among all the considered schemes, validating its effectiveness.

## 6 Conclusion

This paper studied the resolution-aware beam scanning for joint detection and communication in ISAC systems, where the sequential scanning beams were designed with sensing resolution and detection probability requirements. A BCD-based optimization framework was proposed to maximize the average sum rate with guaranteed requirements on resolution and detection probability by optimizing the transmit information beam, radar covariance matrix, and receive beamformer. To address the intractable non-convex design problem, we proposed a low-complexity BCD-based algorithm with SCA, S-procedure, SDR, and series transformations. Simulation results validate the effectiveness of the proposed design. It was shown that the proposed design can provide satisfactory communication performance with stringent detection requirements. Compared with existing studies, the proposed beamwidth controlling method achieved significant performance improvement by fully utilizing the DoFs offered by all antennas. In ISAC systems, random signals are meritable for communication purposes [50]. As a result, the extension of this work to consider random signals constitutes an interesting topic for future work.

**Acknowledgements** This work was supported in part by National Key R&D Program of China (Grant No. 2024YFE0200102).

**References**


1 Liu F, Masouros C, Li A, et al. MU-MIMO communications with MIMO radar: from co-existence to joint transmission. IEEE Trans Wireless Commun, 2018, 17: 2755–2770
2 Liu F, Masouros C, Petropulu A P, et al. Joint radar and communication design: applications, state-of-the-art, and the road ahead. IEEE Trans Commun, 2020, 68: 3834–3862
3 Wu Q, Xu J, Zeng Y, et al. A comprehensive overview on 5G-and-beyond networks with UAVs: from communications to sensing and intelligence. IEEE J Sel Areas Commun, 2021, 39: 2912–2945
4 Yuan W, Wei Z, Li S, et al. Integrated sensing and communication-assisted orthogonal time frequency space transmission for vehicular networks. IEEE J Sel Top Signal Process, 2021, 15: 1515–1528
5 Ouyang C, Liu Y, Yang H. Performance of downlink and uplink integrated sensing and communications (ISAC) systems. IEEE Wireless Commun Lett, 2022, 11: 1850–1854
6 Dong F, Liu F, Xiong Y, et al. Communication-assisted sensing systems: fundamental limits and ISAC waveform design. 2024. ArXiv:2409.03561
7 Xu D, Xu Y, Zhang X, et al. Interference mitigation for network-level ISAC: an optimization perspective. IEEE Commun Mag, 2024, 62: 28–34
8 Xu Y, Xu D, Song S. Sensing-assisted robust SWIPT for mobile energy harvesting receivers in networked ISAC systems. IEEE Trans Wireless Commun, 2025, 24: 2094–2109
9 Dong F, Liu F, Cui Y, et al. Sensing as a service in 6G perceptive networks: a unified framework for ISAC resource allocation. IEEE Trans Wireless Commun, 2022, 22: 3522–3536
10 Xu Y, Zheng M, Xu D, et al. Sensing-aided near-field secure communications with mobile eavesdroppers. 2024. ArXiv:2408.13829
11 Zhou Z C, Liu B, Shen B S, et al. Doppler-resilient waveform design in integrated MIMO radar-communication systems. Sci China Inf Sci, 2024, 67: 112301

12 Xu Y, Xu D, Xie L, et al. Joint BS selection, user association, and beamforming design for network integrated sensing and communication. In: Proceedings of IEEE Global Communications Conference, Kuala Lumpur, 2023. 3111–3117
13 Galappaththige D, Zargari S, Tellambura C, et al. Near-field ISAC: beamforming for multi-target detection. IEEE Wireless Commun Lett, 2024, 13: 1938–1942
14 Su N, Liu F, Masouros C. Secure radar-communication systems with malicious targets: integrating radar, communications and jamming functionalities. IEEE Trans Wireless Commun, 2020, 20: 83–95
15 Li P, Niu Y, Wu H, et al. Secure high-speed train-to-ground communications through ISAC. IEEE Int Things J, 2024, 11: 31235–31248
16 Chiani M, Giorgetti A, Paolini E. Sensor radar for object tracking. Proc IEEE, 2018, 106: 1022–1041
17 Wang Y, Luo H, Gao F, et al. Dynamic target sensing for ISAC systems in clutter environment. In: Proceedings of IEEE Wireless Communications and Networking Conference (WCNC), Dubai, 2024. 1–6
18 Skolnik M I. Introduction to Radar Systems. New York: McGraw-Hill, 1980
19 Xu D, Yu X, Ng D W K, et al. Robust and secure resource allocation for ISAC systems: a novel optimization framework for variable-length snapshots. IEEE Trans Commun, 2022, 70: 8196–8214
20 Wang L, Zhang Y, Shan H, et al. Performance analysis and optimization of ISAC vehicular networks with 360° radar detection. In: Proceedings of IEEE/CIC International Conference on Communications in China (ICCC), Denver, 2024. 580–585
21 Pang X, Guo S, Tang J, et al. Dynamic ISAC beamforming design for UAV-enabled vehicular networks. IEEE Trans Wireless Commun, 2024, 23: 16852–16864
22 Du Z, Liu F, Yuan W, et al. Integrated sensing and communications for V2I networks: dynamic predictive beamforming for extended vehicle targets. IEEE Trans Wireless Commun, 2022, 22: 3612–3627
23 Bai Z, Zhang J, Ouyang Q, et al. An energy-efficient ISAC beam management scheme in UAV communications. In: Proceedings of IEEE Wireless Communications and Networking Conference (WCNC), Dubai, 2024. 1–6
24 Pradhan C, Chen H, Li Y, et al. Joint beamwidth and energy optimization for multi-user millimeter wave communications. In: Proceedings of IEEE International Conference on Communications Workshops (ICC Workshops), Kansas City, 2018. 1–6
25 Luo H, Liu R, Li M, et al. RIS-aided integrated sensing and communication: joint beamforming and reflection design. IEEE Trans Veh Technol, 2023, 72: 9626–9630
26 Wu W, Wang B, Zeng Y, et al. Robust secure beamforming for wireless powered full-duplex systems with self-energy recycling. IEEE Trans Veh Technol, 2017, 66: 10055–10069
27 Wunder G, Schreck J, Jung P, et al. A new robust transmission technique for the multiuser MIMO downlink. In: Proceedings of IEEE International Symposium on Information Theory, Austin, 2010. 2123–2127
28 Wei Z, Liu F, Liu C, et al. Integrated sensing, navigation, and communication for secure UAV networks with a mobile eavesdropper. IEEE Trans Wireless Commun, 2023, 23: 7060–7078
29 Zhang Z, Chen W, Wu Q, et al. Intelligent omni surfaces assisted integrated multi-target sensing and multi-user MIMO communications. IEEE Trans Commun, 2024, 72: 4591–4606
30 Liu R, Li M, Liu Q, et al. SNR/CRB-constrained joint beamforming and reflection designs for RIS-ISAC systems. IEEE Trans Wireless Commun, 2024, 23: 7456–7470
31 van Trees H L. Optimum Array Processing: Part IV of Detection, Estimation, and Modulation Theory. Hoboken: John Wiley & Sons, 2002
32 Liu F, Cui Y, Masouros C, et al. Integrated sensing and communications: toward dual-functional wireless networks for 6G and beyond. IEEE J Sel Areas Commun, 2022, 40: 1728–1767
33 Ren Z, Qiu L, Xu J. Optimal transmit beamforming for secrecy integrated sensing and communication. In: Proceedings of IEEE International Conference on Communications, Seoul, 2022. 5555–5560
34 Richards M A. Fundamentals of Radar Signal Processing. New York: McGraw-Hill, 2005
35 Fishler E, Haimovich A, Blum R S, et al. Spatial diversity in radars-models and detection performance. IEEE Trans Signal Process, 2006, 54: 823–838
36 Ren Z, Xu J, Qiu L, et al. Secure cell-free integrated sensing and communication in the presence of information and sensing eavesdroppers. IEEE J Sel Areas Commun, 2024, 42: 3217–3231
37 Gharavol E A, Larsson E G. The sign-definiteness lemma and its applications to robust transceiver optimization for multiuser MIMO systems. IEEE Trans Signal Process, 2012, 61: 238–252
38 Cox H, Zeskind R, Owen M. Robust adaptive beamforming. IEEE Trans Acoust Speech Signal Process, 1987, 35: 1365–1376
39 Boyd S, Vandenberghe L. Convex Optimization. Cambridge: Cambridge University Press, 2004
40 Grant M, Boyd S. CVX: Matlab software for disciplined convex programming. Version 2.2. 2020. https://cvxr.com/cvx
41 Xu D, Yu X, Sun Y, et al. Resource allocation for IRS-assisted full-duplex cognitive radio systems. IEEE Trans Commun, 2020, 68: 7376–7394
42 Dinh Q T, Diehl M. Local convergence of sequential convex programming for nonconvex optimization. In: Proceedings of Belgian-French-German Conference on Optimization, Berlin, 2010. 93–102
43 Razaviyayn M, Hong M, Luo Z Q. A unified convergence analysis of block successive minimization methods for nonsmooth optimization. SIAM J Optim, 2013, 23: 1126–1153
44 Arora S, Barak B. Computational Complexity: A Modern Approach. Cambridge: Cambridge University Press, 2009
45 Pólik I, Terlaky T. Interior point methods for nonlinear optimization. In: Nonlinear Optimization. Berlin: Springer, 2010. 215–276
46 Xu D, Xu Y, Wei Z, et al. Sensing-enhanced secure communication: joint time allocation and beamforming design. In: Proceedings of the 21st International Symposium on Modeling and Optimization in Mobile, Ad Hoc, and Wireless Networks (WiOpt), Singapore, 2023. 673–680
47 Ren Z, Qiu L, Xu J, et al. Robust transmit beamforming for secure integrated sensing and communication. IEEE Trans Commun, 2023, 71: 5549–5564
48 Jiang T, Jin M, Guo Q, et al. Full-duplex ISAC-enabled D2D underlaid cellular networks: joint transceiver beamforming and power allocation. 2024. ArXiv:2408.11329
49 Xu D, Khalili A, Yu X, et al. Integrated sensing and communication in distributed antenna networks. In: Proceedings of IEEE International Conference on Communications Workshops (ICC Workshops), Rome, 2023. 1457–1462
50 Lu S, Liu F, Dong F, et al. Random ISAC signals deserve dedicated precoding. IEEE Trans Signal Process, 2024, 72: 3453–3469


## Appendix A

Scaling $\boldsymbol{u}[l]$ with any arbitrary constant will not alter the value of the objective function in (26). Hence, the optimization problem in (26) can be reformulated as [38]

$$\underset{\boldsymbol{u}[l]}{\text{minimize}} \;\; \boldsymbol{u}^{\mathrm{H}}[l]\boldsymbol{F}[l]\boldsymbol{u}[l]$$

$$\mathrm{s.\,t.}\quad \boldsymbol{u}^{\mathrm{H}}[l]\boldsymbol{a}(\phi_l) = 1. \tag{A1}$$

The Lagrangian function of the optimization problem in (A1) is given by

$$\mathcal{G}(\boldsymbol{u}[l], \lambda) = \boldsymbol{u}^{\mathrm{H}}[l]\boldsymbol{F}[l]\boldsymbol{u}[l] + \lambda(\boldsymbol{u}^{\mathrm{H}}[l]\boldsymbol{a}(\phi_l) - 1), \tag{A2}$$

where $\lambda$ is the Lagrange multiplier. According to the Karush-Kuhn-Tucker (KKT) condition [39], we have

$$\begin{cases} \dfrac{\partial \mathcal{G}}{\partial \boldsymbol{u}[l]} = 2\boldsymbol{F}[l]\boldsymbol{u}[l] + \lambda \boldsymbol{a}(\phi_l) = \boldsymbol{0}, \\ \boldsymbol{u}^{\mathrm{H}}[l]\boldsymbol{a}(\phi_l) = 1. \end{cases} \tag{A3}$$

By solving the KKT condition, we can obtain the optimal $\boldsymbol{u}[l]$ as

$$\boldsymbol{u}^*[l] = \frac{\boldsymbol{F}^{-1}[l]\boldsymbol{a}(\phi_l)}{\boldsymbol{a}^{\mathrm{H}}(\phi_l)\boldsymbol{F}^{-1}[l]\boldsymbol{a}(\phi_l)}. \tag{A4}$$